Fast, robust and efficient 2D pattern recognition for re-assembling fragmented images

Massimo Fornasier [b] Domenico Toniolo* [a]

[a] *Dipartimento di Fisica "G. Galilei"*
Università degli Studi di Padova, Via F. Marzolo 8, I-35131 Padova - ITALY
Tel +39 049 8277081, Fax +39 049 8277102
email: toniolo@pd.infn.it

[b] *Dipartimento di Metodi e Modelli Matematici per le Scienze Applicate*
Università "La Sapienza" di Roma, Via A. Scarpa 16/B, I-00161 Roma - ITALY
email: mfornasi@math.unipd.it

Abstract

We discuss the realization of a fast, robust and accurate pattern matching algorithm for comparison of digital images implemented by discrete Circular Harmonic expansions based on sampling theory. The algorithm and its performance for re-assembling fragmented digital images are described in detail and illustrated by examples and data from the experimentation on an art fresco real problem. Because of the huge database of patterns and the large scale dimension, the results of the experimentation are relevant to describe the power of discrimination and the efficiency of such method.

Key words: art fresco reconstruction, Circular Harmonic expansions, pattern recognition, rotation invariance, fast computation, sampling theory
Classification: 42C15, 65T50, 68Q25, 68T10, 68U10, 94A08, 94A20

[1] The work of M.F. has been developed during his Doctorate in Computational Mathematics at the Department of Pure and Applied Mathematics of the University of Padova - ITALY. He also acknowledges the financial support provided through the European Union's Human Potential Programme, under contract HPRN-CT-2002-00285 (HASSIP).
[2] The experimental part of this work has been supported by Fondazione Cassa di Risparmio di Padova e Rovigo, in agreement with Soprintendenza al Patrimonio Storico Artistico e Demoetnoantropologico del Veneto - Italy.

1 Introduction

Since 1994 the authors have been involved in the fascinating attempt to recall to life a very important Italian art fresco (A. Mantegna, Cappella Ovetari, Chiesa degli Eremitani in Padova), fragmented in thousands of pieces by an Allied bombing in the Second World War (1944) [15,16,10]. Recently a digital cataloging of the fragment images made possible to count their exact number (80735). The distribution of the areas shows that most are relatively small, with an average surface area of 5-6 square centimeters, a total area of 77 square meters versus an original surface of several hundreds square meters. These a priori data demonstrated the lack of continuous fragments for any given fragment and makes extremely improbable that any reconstruction will be successful using methods based on the outline shape of the fragments. There is no information on the possible location of the pieces on the huge original surface and it is unknown also the angle of rotation with respect to the original orientation. Some fairly good quality black and white photographs from between 1900 and 1920 exist, but they suffer from non-linear spectral distortion. A more detailed and complete description of the problem can be found in the contribution [25].
These facts impose that any feasible computer based solution for a possible recomposition by comparison of the fragments and the fresco digital gray images must be

- *fast*, because of the huge number of fragments and original surface of the fresco;
- *robust*, because of the strong noise presence and intrinsic differences between the images, due to the damage of the bomb and the different photographic techniques;
- *accurate*, because of the fairly small dimensions of the fragments;
- *translation-rotation invariant*, because of the unknown original location and orientation of the fragments.

The request of a fast algorithm excludes the implementation of any comparison *pixel-by-pixel* and suggests that methods based on (compressed) series expansions can be more efficient. Besides other classical expansions, like Laguerre-Gauss [7] or Zernike polynomials [18] (fairly difficult to implement numerically), Circular Harmonic decompositions have found a relevant role in pattern matching because of their rotation invariance (self-steerable) properties and their effective and successful optical implementations [3–6]. In this paper, we want to present a digital/numerical implementation of compactly supported Circular Harmonics and an effective 2D pattern recognition algorithm, based on these discrete expansions, which fulfills all the required properties listed above. The algorithm and its performance are described in detail and illustrated by examples and data from the experimentation on the fresco

real problem. Because of the huge database of patterns and the large scale dimension, the results of the experimentation are relevant to describe the power of discrimination and the efficiency of such method. Other problems can be interpreted in such a picture: experiments in character recognition, motion field detection and local rotation registration have also given very good results.

In literature other kind of expansions have been presented as possible tools for pattern matching: to cite some, 2D (Circular Harmonic) wavelets [1,2,24] and multiscale self-steerable pyramid decompositions [22,23]. Even if they have given very interesting and promising results on small scale and local registration problems, it is still difficult to implement algorithms where a reasonable and feasible compromise among speed, robustness and location-rotation resolution can be realized on large scales.

The paper is organized as follows: Section 2 illustrates the Circular Harmonic expansions and their properties. In particular, it is shown that the moments constructed by correlation of a signal with the Circular Harmonic system is a total information that can be used then for a complete comparison with an other signal. We discuss the discrete implementation of Circular Harmonic expansions by sampling and we will show that, up to limit the system to a suitable and computable finite number of elements, one can efficiently calculate the moments and preserve with optimal approximation *completeness, local orthonormality* and *self-steerability* also in the discrete domain. Section 3 illustrates the pattern recognition algorithm and its complexity is discussed with respect to a reference optimal method. In Section 4 numerical results and stability in real cases are presented and compared with the reference optimal method. An appendix collects notations and the relevant result in *aliasing error analysis* in sampling theory we have used for the efficient discretization of the Circular Harmonic system.

2 Discrete compactly supported Circular Harmonics

Compactly supported Circular Harmonics (CH) arise as natural solutions of the Laplace eigenvalues problem on a disk under Dirichlet conditions [27], and they are related to relevant physical problems with rotation invariant symmetries. In fact, since the Laplacian commutes with rotations, CH are also eigenfunctions of any rotation operator.

We denote in the following $L^p(\Omega)$ the Lebesgue space of p-summable functions on $\Omega \subset \mathbb{R}^d$. Assume $\Omega_a \subset \mathbb{R}^2$ is a disk of radius $a > 0$. The system of Circular Harmonic functions on Ω_a is defined in polar coordinates by

$$e_{m,n,a}(r,\theta) = \frac{c_{m,n}}{a} J_m(j_{m,n} r/a) e^{im\theta}, \quad m \in \mathbb{Z}, \quad n \in \mathbb{N}, \tag{1}$$

$$c_{m,n} = \pi^{-\frac{1}{2}}[\frac{dJ_m(s)}{ds}|_{s=j_{m,n}}]^{-1}, \tag{2}$$

where J_m's are Bessel functions of the first kind of order $m \in \mathbb{Z}$, $(j_{m,n})_{n\in\mathbb{N}}$ is the sequence of their positive zeros [26], and $c_{m,n}$ is a normalization constant. We summarize their properties:

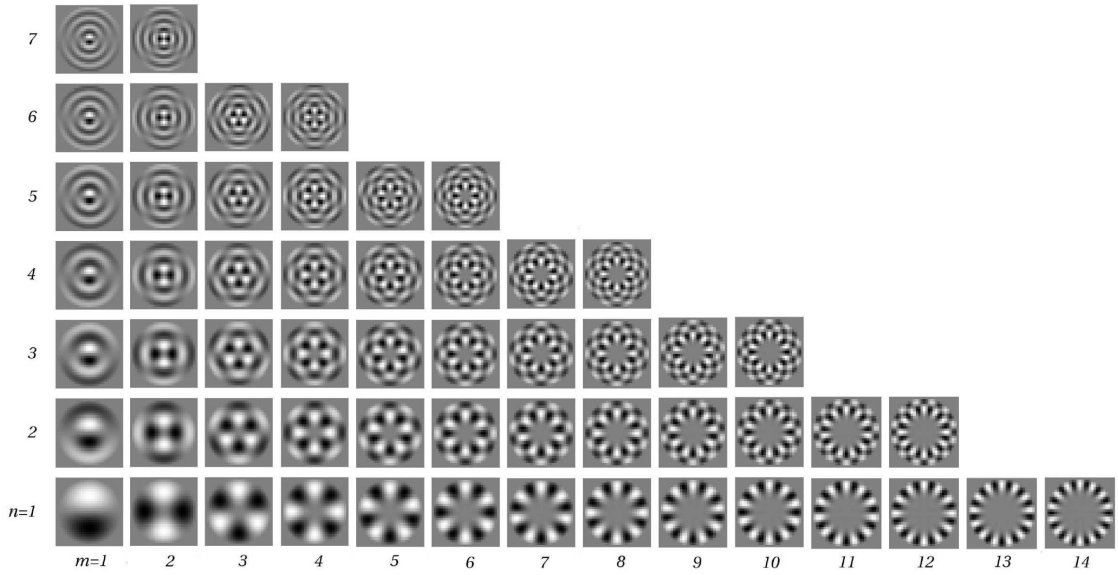

Fig. 1. Compactly supported CH

i) CH constitute an orthonormal basis for $L^2(\Omega_a)$ [27], i.e.,

$$\langle e_{m,n,a}, e_{m',n',a}\rangle := \int_{\Omega_a} e_{m,n,a}(x)\overline{e_{m',n',a}(x)}dx = \delta_{(m,n),(m',n')},$$

being $\overline{f(x)}$ the complex conjugate of $f(x)$, and solve the Laplace eigenvalues problem:

$$\begin{cases} e_{m,n,a} \in H_0^1(\Omega_a) \cap C^\infty(\overline{\Omega_a}), \\ \Delta e_{m,n,a} = -\left(\frac{j_{m,n}}{a}\right)^2 e_{m,n,a}, \\ e_{m,n,a}(x) = 0, \forall x \in \partial\Omega_a, \end{cases} \tag{3}$$

where $H_0^1(\Omega_a)$ is the Sobolev space of functions vanishing on the border $\partial\Omega_a$.

ii) CH are characterized by special frequencies: in fact, each $e_{m,n,a}$ is dominated by a particular set of frequencies related to $j_{m,n}/a$. The *Fourier transform*

of a summable function f on $\mathbb{R}^d$ is

$$\mathcal{F}f(\omega) = \int_{\mathbb{R}^d} f(x) e^{-2\pi i \langle \omega, x \rangle_{\mathbb{R}^d}} dx,$$

where $\langle \cdot, \cdot \rangle_{\mathbb{R}^d}$ is the scalar product in $\mathbb{R}^d$. In particular, the Fourier transform $\mathcal{F}e_{m,n,a} \in L^1(\mathbb{R}^2)$ and has quite fast decay ($\mathcal{F}e_{m,n,a}(r,\theta) \sim r^{-5/2}$, see Fig. 2 and [27,10]). This property is relevant to ensure that CH produce relatively small *aliasing errors* [21] once they are sampled as we will discuss in the following. In particular, the CH basis minimizes aliasing errors among all the possible Fourier-Dini bases which are solutions of the Laplace eigenvalue problem (with Neumann conditions) [27,10], because in general the latter have slower Fourier transform decay.

iii) Let R_α be the rotation operator of angle α, i.e., in polar coordinates $R_\alpha f(r,\theta) = f(r, \theta + \alpha)$, for all functions f on Ω_a. Then CH are eigenfunctions of any rotation operator (*self-steerability*) [5]

$$R_\alpha e_{m,n,a} = e^{im\alpha} \cdot e_{m,n,a}, \tag{4}$$

for all $m \in \mathbb{Z}, n \in \mathbb{N}$, and this property is used to detect mutual angles in comparisons of digital images, as we will discuss in the following.

2.1 Analysis and synthesis of an image by CH expansions

We describe in this section how moments computed by correlation with respect to CH can be used for a complete analysis of 2D (digital) signals.

For all images $f \in L^2(\mathbb{R}^2)$, the moment (or *Circular Short Time Fourier Transform (CSTFT)* [9,17])

$$\mathcal{F}_{CSTFT}(f)(x,m,n) = \langle f, e_{m,n,a}(\cdot - x) \rangle_{L^2} = \int_{\mathbb{R}^2} f(y) \overline{e_{m,n,a}(y-x)} dy, \tag{5}$$

localizes f at the space point $x \in \mathbb{R}^2$ and at the frequency $j_{m,n}/a$. As we write $\tau > 0$ we mean $\tau = (\tau_1, ..., \tau_d) \in \mathbb{R}^d_+$ and we denote $det(\tau) = \tau_1 ... \tau_d$. The multiplication of two vectors $x, y \in \mathbb{R}^d$ is assumed componentwise $x \cdot y := xy := (x_1 y_1, ..., x_d y_d)$.

There exists $\tau = \tau(a) > 0$, depending on $a > 0$, such that $\mathbb{R}^2 = \bigcup_{k \in \mathbb{Z}^d} \tau k + \Omega_a$. Therefore, by application of [11, Theorem 1] the sequence $(e_{m,n,a}(\cdot - \tau k))_{k,m,n}$ is a global *frame* for $L^2(\mathbb{R}^2)$ (see [8] for an introduction on frames) generated by the local orthonormal basis $(e_{m,n,a})_{m,n}$ on the disk. One can invert (5) by

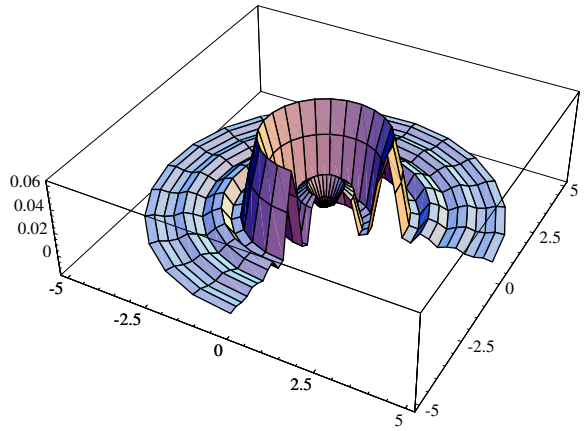

Fig. 2. Absolute value of the Fourier transform of a compactly supported CH. The dominant frequencies $j_{m,n}/a$ and the fast decay are visualized.

using the *canonical dual frame* $(\widetilde{\mathcal{E}}_{m,n,a,k})_{m,n,k}$ [8,11,14]:

$$f = \sum_{k,m,n} \mathcal{F}_{CSTFT}(f)(\tau k, m, n)\widetilde{\mathcal{E}}_{m,n,a,k} \tag{6}$$

This means in particular that the sequence $(\mathcal{F}_{CSTFT}(f)(\tau k, m, n))_{k,m,n}$ is a *complete information on the signal* f and then can be used for a complete comparison with an other signal.

We show in the following how to compute the $\mathcal{F}_{CSTFT}$ in a *fast and accurate* way and how to discretize formula (5) for use in applications. For functions (on continuous or discrete domain) f, g, h we define $I(h)(x) = \overline{h(-x)}$ the involution operator and with $f * g$ the convolution operator of f and g.

It is not hard to see that $\mathcal{F}_{CSTFT}(f)(\tau k, m, n) = (f * I(e_{m,n,a}))(\tau k)$. Hence, one can consider to implement an FFT (Fast Fourier Transform) convolution at the resolution τ to compute $\mathcal{F}_{CSTFT}(f)(\tau k, m, n)$. This choice produces the following approximation:

$$\mathcal{F}_{CSTFT}(f)(\tau k, m, n) \approx det(\tau) \sum_{l \in \mathbb{Z}^2} f(\tau l)\overline{e_{m,n,a}(\tau(l-k))} \tag{7}$$

As we have fixed τ, we will write l^2 instead of $l^2(\tau\mathbb{Z}^d)$ the space of discrete signals with finite energy and we will suppose it endowed with the scalar product $\langle f, g\rangle_{l^2} \equiv det(\tau)\sum_{k\in\mathbb{Z}^d} f(\tau k)\overline{g(\tau k)}$. If f is a discrete signal then we will denote with $\mathcal{F}f$ or $\hat{f}$ also the *discrete Fourier transform* of f.

Observe that $\langle f, e_{m,n,a}(\cdot - \tau k)\rangle_{l^2} = det(\tau)\sum_{l\in\mathbb{Z}^2} f(\tau l)\overline{e_{m,n,a}(\tau(l-k))}$. It is known that scalar products are preserved under suitable sampling whenever

the signals involved are band-limited. Thus in such case formula (7) is exact and no approximation is appearing.

In the case of non band-limited signals, *aliasing errors* [21,12] propagate to scalar products and perturb the approximation. In order to minimize the approximation error in (7) one should consider only those Circular Harmonic functions for which the aliasing errors are small. In Appendix, Theorem 3 describes how to measure aliasing errors of a function f by suitable *function space norms* of the "tails" of the Fourier transform of f and how to optimize the approximation (7) for all possible choices of f: one should select those CH which minimize this norm (as the measure of their aliasing error). In practice, one discretizes the infinite frame $(e_{m,n,a}(\cdot - \tau k))_{m,n,k}$ by sampling it on $\tau\mathbb{Z}^2$ and by selecting only a finite number of elements which guarantee a good approximation. This selection produces a finite sampled sequence (the "$\cdot^s$" stands for "sampled") $(e^s_{m,n,a}(\cdot - \tau k))_{k,m,n}$ that is again a global (discrete) frame for $l^2(\tau\mathbb{Z}^2)$: hence *no truncation error occurs* when one wants to reproduce even a discrete signal from (7). By formula (27) one can show, numerically but also analytically [10], that for any precision $\varepsilon > 0$ and all radius $a > 0$ there exist a resolution $\tau = \tau(a) > 0$ and a *frequency set* $\Phi_{a,\varepsilon}$ of couples (m, n) such that for $(m, n) \in \Phi_{a,\varepsilon}$, the corresponding $e_{m,n,a}$ *minimizes the aliasing error up to* ε. In order to select a suitable method in concrete cases, we observe that the images, divided between channels (RGB or gray levels) can be considered as functions with real values. Since for any real signal h, $\langle h, e_{-m,n,a}\rangle = (-1)^m\overline{\langle h, e_{m,n,a}\rangle}$ [26,27], the terms with $m < 0$ of the $\Phi_{a,\varepsilon}$ are redundant and maybe deduced from that part of $\Phi_{a,\varepsilon}$ with $m > 0$. Hence, we avoid consideration of $e_{-m,n,a}$ for $m > 0$, obtaining a reduction by half of the calculation time.

Because of the peculiar shape of $\mathcal{F}e_{m,n,a}$, i.e., absolute radial and dominant frequencies at $j_{m,n}/a$ and vanishing residual tails (Fig. 2), practically one can select with good approximation $(m, n) \in \Phi_{a,\varepsilon}$ whenever $j_{m,n} \leq \frac{2\pi a}{\tau}\varepsilon^{1/2}$. In Fig. 1 and 3 we show some examples of an admissible frequency set $\Phi_{a,\varepsilon}$.

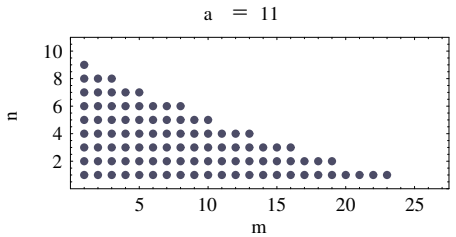

Fig. 3. Example of the set $\Phi_{a,\varepsilon}$ described by $j_{m,n} \leq \frac{2\pi a}{\tau}\varepsilon^{1/2}$ for $\varepsilon = 0.1$.

Therefore, for a suitable choice of $\varepsilon > 0$, one can in particular ensure that

- The sequence $(e^s_{m,n,a})_{(m,n)\in\Phi_{a,\varepsilon}}$ is *almost* orthonormal,

$$\delta_{(m',n'),(m,n)} = \langle e_{m',n',a}, e_{m,n,a}\rangle \approx \langle e^s_{m',n',a}, e^s_{m,n,a}\rangle_{l^2}. \tag{8}$$

  As a consequence the finite sequence $(e^s_{m,n,a})_{(m,n)\in\Phi_{a,\varepsilon}}$ is linearly independent and $\#\Phi_{a,\varepsilon} = \#\Omega_a$, then $(e^s_{m,n,a})_{(m,n)\in\Phi_{a,\varepsilon}}$ is a local frame for $l^2(\Omega^s_a)$ with $(e^s_{m,n,a}(\cdot - \tau k))_{k,(m,n)\in\Phi_{a,\varepsilon}}$ as respective *discrete* global frame for $l^2(\tau\mathbb{Z}^2)$ [11,14], and the discrete moments (7) are again a complete information.
- The discrete compactly supported CH approximatively satisfies (4) in weak sense. This means that, for any R_α rotation operator, one has

$$\begin{aligned} &\langle (R_\alpha f)^s, e^s_{m,n,a}\rangle_{l^2} \approx \langle R_\alpha f, e_{m,n,a}\rangle = \\ &= \langle f, R_{-\alpha} e_{m,n,a}\rangle \approx e^{im\alpha}\langle f^s, e^s_{m,n,a}\rangle_{l^2}. \end{aligned} \tag{9}$$

3 2D pattern recognition algorithms

We illustrate in this section an efficient pattern matching algorithm based on the CH-moments $\mathcal{F}_{CSTFT}$. We refer the properties of the method directly to the application on the computer-based recomposition of frescoes, where one would like to localize the images of some fragments on an "old" picture of the fresco prior to damage. However, the resulting method can be efficiently applied in other situations where one wants to detect a small particular in a larger image up to mutual rotation.

Digital images can be represented by matrices and we consider all the following signals sampled at some fixed resolution τ (without loss of generality one can assume $\tau = 1$) and we identify them with their sampling matrix. According to the considerations mentioned above, an image supported on a discrete disk of radius $a > 0$ can be represented on a finite dimension space, identified by the set $\Phi_{a,\varepsilon}$. This space has an *almost* orthonormal basis consisting of sampled eigenfunctions of rotation operators (8). The choice of this space also guarantees that the passage from the continuous to the discrete domain is (almost) error free in angle resolution (9).

3.1 Matching coefficient up to rotation

An *ideal method* of comparison is realized by rotating one image with respect to the other and by detecting the rotation angle which performs the best possible matching, in some measure. Given a CH expansion of an image, one can rotate it just multiplying the moments in a suitable way by eigenvalues

Fig. 4. Fragment of the Andrea Mantegna's fresco, bombed in 1944, over the correspondent old gray photo dated to 1920.

of the rotation operator (9):

$$f = \sum_{m,n} f_{m,n} e_{m,n,a}, \quad R_\theta f \approx \sum_{m,n} e^{im\theta} f_{m,n} e_{m,n,a}, \tag{10}$$

where $f_{m,n} = \langle f, e_{m,n,a} \rangle_{l^2}$. The approximation symbol "$\approx$" is due to the *aliasing errors* which are in practice negligible, as we have discussed in the previous section. Given two images f and g (defined on a disk) one can define the *matching coefficient* of the signals f and g, depending on the rotation, given by:

$$M(f, g, \theta) := \frac{\langle R_\theta f, g \rangle_{l^2}}{\|f\|_2 \|g\|_2} \approx \frac{1}{\|f\|_2 \|g\|_2} \sum_{m,n} e^{im\theta} f_{m,n} \overline{g_{m,n}}. \tag{11}$$

This formula is equivalent to measure the angle between $\frac{R_\theta f}{\|f\|_2}$ and $\frac{g}{\|g\|_2}$ as unitary vectors in the finite dimension CH space, indexed by the set $\Phi_{a,\varepsilon}$.

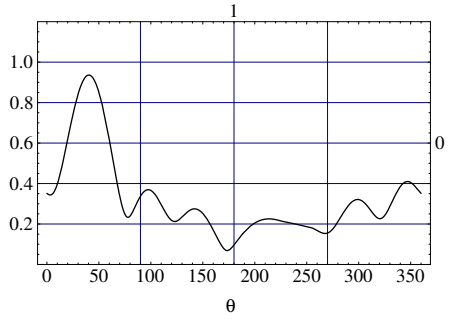

Fig. 5. $|M(f,g,\theta)|$ for $\theta \in [0°, 360°)$. The maximum is realized at $\alpha \approx 40°$

The angle α such that $|M(f,g,\alpha)| = \max_{\theta\in[0,2\pi)} |M(f,g,\theta)|$ is an optimal angle which realizes the best matching (Fig. 5). Let us call this strategy *optimal matching procedure*. In fact, $0 \leq |M(f,g,\theta)| \leq 1$ and it is $|M(f,g,\theta)| = 1$ if and only if $f = \lambda g$ up to rotation of θ, and $\lambda > 0$. Hence the matching coefficient is independent on *contrast* in the sense that if $\lambda > 0$ then $M(\lambda f, g, \theta) = M(f,g,\theta)$ [4].

3.2 Computational cost

A direct computation of the maximum of $M(f,g,\theta)$ is quite expensive to achieve good accuracy, because one needs high sampling rate in angle resolution. Hence, it is time consuming and it requires the use of much memory to store all coefficients involved in formula (11) for all the possible positions and angles.

In order to establish a comparison of efficiency with the novel algorithm we are going to illustrate later in this paper, let us estimate here which is the computational cost of the optimal matching procedure. Assume that the sampled Circular Harmonic functions and that the moments $g_{m,n}$ for all the positions are pre-calculated. Denote with $C(\Gamma)$ the number of complex operations to compute the quantity Γ. Because of (8) if $(m,n) \in \Phi_{a,\varepsilon}$ then one can estimate $m \lesssim 2a$ and $n \lesssim a$ and $\#\Phi_{a,\varepsilon} \sim a^2$. As a consequence, it is not difficult to see that $C(f_{m,n}) \sim \pi a^2$ and $C(M(f,g,\theta)) \sim 3a^2$. One should multiply this last factor by the number N_{rot} of rotations to be considered, as a relevant constant, and then apply an optimization to detect the best angle α: the complexity of the *Quick Sort algorithm* is $O(N\log(N))$ and hence, one has $C(M(f,g,\alpha)) \sim 3N_{rot}a^2 + \alpha_{QS}N_{rot}\log(N_{rot})$. Since the calculation should be executed for all relevant positions of a given $h \times w$ reference image (one should consider all the positions which are in the interior of the reference image excluding a frame of width a), one finally achieves that to compute the

best position one should execute c.a.

$$\pi a^4 + (h-a)(w-a)(3N_{rot}a^2 + \alpha_{QS}N_{rot}\log(N_{rot})) +$$

$$+\alpha_{QS}(h-a)(w-a)\log((h-a)(w-a))$$

complex operations. Observe that for a given radius $a > 0$, to achieve an accuracy comparable with the resolution of the sampling lattice, a suitable choice of N_{rot} is $\sim 2\pi a$.

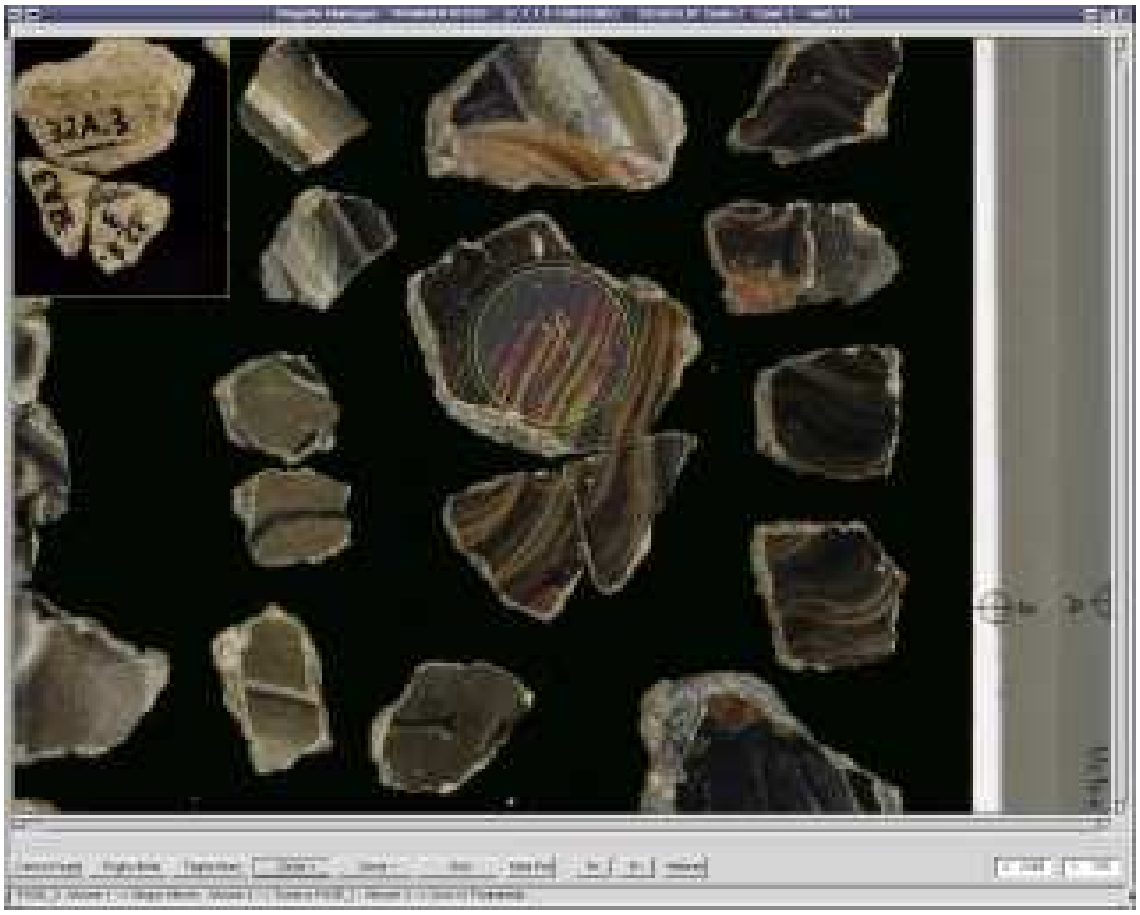

Fig. 6. The figure shows a sheet from the digital catalogue of fragment images. In particular a disk portion is extracted from a fragment to be processed for the localization.

3.3 The circular sum procedure of computation of $M(f, g, \alpha)$

We want to show here a new procedure of calculation of the matching coefficient, invariant under rotation, by means of a *sequential (memory saving)* and *faster (FFT based)* comparison of CH-moments where the angle is detected by *implicit* computations. We will show that using this procedure the computational cost can be dramatically reduced in the range of parameters used in

concrete applications. We pretend also that this novel method of comparison can be as effective and robust as the ideal one, at least for a reasonable class of cases.

If $\widetilde{f}$ is a disk extracted from a fragment (Fig. 6), and f its image under rotation by $-\alpha$ in such a way as to return it to its original orientation, then by (10)

$$\widetilde{f} \approx \sum_m \sum_n e^{im\alpha} f_{m,n}\, e_{m,n,a} = \sum_m f_m, \tag{12}$$

where $f_m = \sum_n e^{im\alpha} f_{m,n}\, e_{m,n,a}$ and $(m,n) \in \Phi_{a,\varepsilon}$. If $g_{i,j}$ represents a disk extracted around any position (i,j) of the fresco image G, we could write analogously:

$$g_{i,j} = \sum_m g_m^{i,j}, \tag{13}$$

where $g_m^{i,j} = \sum_n g_{m,n}^{i,j}\, e_{m,n,a}$, $g_{m,n}^{i,j} = \langle g_{i,j}, e_{m,n,a} \rangle_{l^2} \approx \mathcal{F}_{CSTFT}(G)(i,j,m,n)$.

In the following, we assume componentwise operations on the matrices. We consider, now, a matrix F_m with same dimensions $h \times w$ as G with entries consisting of zeros except for the entries representing f_m, translated *modulo* $h \times w$ so that the center of the disk coincides with the left upper corner of G, considered as the axes origin. As discussed in Section 2 we can execute a fast comparison of the circular harmonics moments by convolutions and the use of the FFT.

Let us denote $F = \sum_m F_m$ and $F_m^*(k) = F_m(-k)$ modulo $h \times w$, for $k = (i,j) \in \mathbb{Z}^2$. According to (8), we have:

$$\begin{aligned} &(F_m^* * G)(i,j) = \langle f_m, g_{i,j} \rangle_{l^2} \approx \\ &\approx \langle f_m, g_m^{i,j} \rangle_{l^2} \approx \textstyle\sum_n e^{im\alpha} f_{m,n} \overline{(g_{m,n}^{i,j})}. \end{aligned} \tag{14}$$

It is well known that a convolution is equivalent to a multiplication in the frequency domain

$$\mathcal{F}^{-1}(\widehat{F_m^*}\widehat{G})(i,j) = (F_m^* * G)(i,j). \tag{15}$$

Even if the $e_{0,n,a}$'s are the only totally rotation invariant components of the expansion, we will define the matching coefficient computation without counting the contribution of the projection on the $e_{0,n,a}$'s. In fact, these components cannot be useful in order to detect mutual angles. Moreover, this choice makes the comparison independent of *brightness*, since $\langle c, e_{m,n,a} \rangle = 0$ for any constant $c > 0$ and $m \neq 0$. Hence, using $m > 0$, one defines inductively the

procedure for an *implicit approximated calculation of optimal matching and angle*: at some $m > 0$, one assumes that a first determination of the optimal angle, say $\alpha_{m-1} \approx \alpha$, is given maybe by means of some calculations on previous coefficients $v_k = \sum_n f_{k,n}\overline{g^{i,j}_{k,n}}$, $k = 1, ..., m-1$. Then one computes a next approximation/correction of the optimal angle using the next independent complex vector v_m, just rotating back it of α_{m-1}, i.e., multiplying v_m by $e^{-i(m-1)\alpha_{m-1}}$, and setting $\alpha \approx \alpha_m = \arg(e^{-i(m-1)\alpha_{m-1}} v_m)$. An initial approximation from which to start can be deduced by v_1 whenever f and $g_{i,j}$ can be "close enough" up to rotation. Formally this can be expressed by the following procedure

$k \in \mathbb{N}\backslash\{0\}$ and $z, v \in \mathbb{C}\backslash\{0\}$.

We consider the binary operator $\oplus_k$ defined by:

$$z \oplus_k v = z + v \left(\frac{z}{|z|}\right)^{1-k}. \tag{16}$$

For $m \in \mathbb{N}\backslash\{0\}$ and $v_1, ..., v_m \in \mathbb{C}\backslash\{0\}$ the *circular sum* of order m is the operator $\bigoplus_{k=1}^m$ defined recursively by:

$$\begin{cases} \bigoplus_{k=1}^m v_k = v_1, & m = 1 \\ \bigoplus_{k=1}^m v_k = (\bigoplus_{k=1}^{m-1} v_k) \oplus_m v_m & m > 1. \end{cases} \tag{17}$$

By induction on formula (17) one can easily show the following formal properties of the circular sum:

for $m \in \mathbb{N}\backslash\{0\}$ let $v_1 = \rho_1 e^{i\alpha}, ..., v_m = \rho_m e^{im\alpha} \in \mathbb{C}\backslash\{0\}$, $\rho_k > 0$ for all $k = 1, .., m$ and $\alpha \in [0, 2\pi)$.

i) (Angle detection property) $\bigoplus_{k=1}^m v_k = e^{i\alpha}\left(\sum_{k=1}^m \rho_k\right)$;

ii) (Angle detection in presence of errors) If $v_{m-1} = \rho_{m-1} e^{i\left((m-1)\alpha + \delta_{\alpha_{m-1}}\right)}$ and $v_m = \rho_m e^{i(m\alpha + \delta_{\alpha_m})}$ then

$$\bigoplus_{k=1}^m v_k = e^{i\alpha}\left(w_{m-1} + \frac{e^{i\delta_{\alpha_m}}\rho_m}{sgn(w_{m-1})^{m-1}}\right), \tag{18}$$

where $w_{m-1} = \sum_{k=1}^{m-2} \rho_k + e^{i\delta_{\alpha_{m-1}}}\rho_{m-1}$. As we will discuss in Section 4 this last property ensures stability in angle resolution also in presence of strong noise, see also Fig. 11.

We are now ready to define the new procedure for computing the matching coefficient.

Fig. 7. Some re-composed fragments are shown on the original background.

With the notation used above, we define the *matching matrix* of f and G by

$$M(F,G) := \frac{1}{\sum_{k=1}^{m} \|f_k\|_2^2} \bigoplus_{k=1}^{m} \frac{\|f_k\|_2}{(\|g_k^{i,j}\|_2)_{i,j}} \mathcal{F}^{-1}(\widehat{F_k^*}\hat{G}), \tag{19}$$

where $\|f_k\|_2$ is the (discrete) norm of f_k, $(\|g_k^{i,j}\|_2)_{i,j}$ is the matrix of the norms of $g_k^{i,j}$ and $m > 0$ is the maximal integer for which there exists $n \in \mathbb{N}$ such that $(m,n) \in \Phi_{a,\varepsilon}$. The circular sum in (19) acts componentwise on the matrices.

For each point (i,j) of the image G, the matching matrix returns the matching coefficient given by $0 < |M(F,G)(i,j)| \leq 1$, measure of the correspondence with the fragment up to relative rotation. In fact, if we suppose there exists a position $(\bar{i},\bar{j})$ in G, such that:

$$g_{\bar{i},\bar{j}} = f, \tag{20}$$

from (14-15) one has

$$\mathcal{F}^{-1}(\widehat{F_k^*}\hat{G})(\bar{i},\bar{j}) \approx e^{ik\alpha}\|f_k\|_2^2, \tag{21}$$

for each k. Hence, by the property (i) of the circular sum, we have:

$$M(F,G)(\overline{i},\overline{j}) \approx \frac{1}{\sum_{k=1}^{m} \|f_k\|_2^2} \bigoplus_{k=1}^{m} e^{ik\alpha} \|f_k\|_2^2 = e^{i\alpha}. \tag{22}$$

We deduce that a necessary condition, so that a position $(\overline{i},\overline{j})$ is the original one of the fragment, is:

$$\begin{cases} |M(F,G)(\overline{i},\overline{j})| \approx 1, \\ \arg(M(F,G)(\overline{i},\overline{j})) \approx \alpha. \end{cases} \tag{23}$$

Up to the negligible aliasing errors, the condition is sufficient, since we have shown that $(\mathcal{F}_{CSTFT}(G)(i,j,m,n))_{i,j,m,n}$ is a complete information.

Of course one can adaptively construct a subset of $\Phi_{a,\varepsilon}$ depending on the particular fragment to *compress* the information used in the calculation of (19), reducing much the computational cost. In practice we have verified that for general fragments most of the energy is concentrated in the lower m-components $m = 1, 2, 3, \ldots$ that can be already enough to have a quite discriminating comparison.

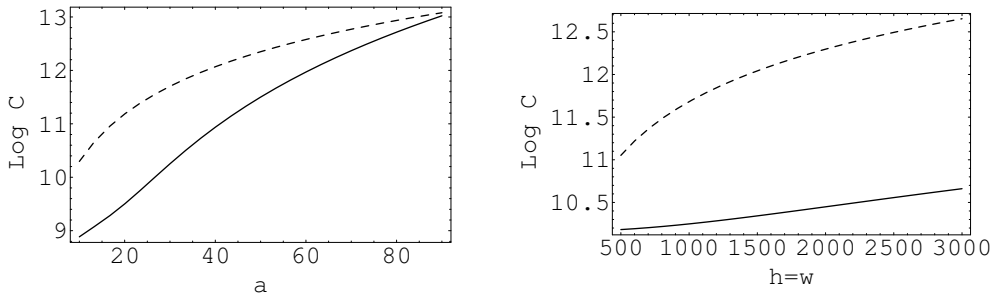

Fig. 8. The computational cost of the optimal matching procedure (dashed curve) and of the circular sum procedure (continuous curve) are shown. With respect to increasing values of radius $6 \leq a \leq 90$ on the left and fixed size $h = w = 1024$, and with increasing values of the dimensions $512 \leq h = w \leq 3000$ and fixed radius $a = 30$ on the right. With radius $a \approx 20$ and size $h = w = 1024$ the cost can be 50 times smaller.

3.4 Computational cost and comparison with the optimal matching procedure

Since $\hat{G}$, and the norms $\|g_k^{i,j}\|_2^2$ can be pre-calculated, the computational cost of the matching matrix depends essentially on the fragment quantities, the

correlation and the cost of the circular sum. By computations in Section 3.2 one has

- $C(F_k) \sim \pi^2 a^5 + \pi a^3$;
- since F is zero except for $2a$ rows/columns one can compute $\widehat{F_k^*}$ in $C(\widehat{F_k^*}) \sim 2a \cdot \alpha_{FFT}(h \log(h) + w \log(w))$ complex operations, by applying the 1D-FFT firstly along the rows and then along the columns;
- $C(\widehat{F_k^*}\hat{G}) \sim h\ w$;
- $C(\mathcal{F}^{-1}(\widehat{F_k^*}\hat{G})) \sim \alpha_{FFT}^2 h\ w \log(h\ w)$;
- $C(\|f_k\|_2^2) \sim 2a$;
- $C(\bigoplus_{k=1}^m v_k) \sim \frac{7m+m^2}{2}$;

From these estimates one shows that

$$C(M(F,G)) \sim 2a(\pi^2 a^5 + \pi a^3 + a \cdot \alpha_{FFT}(h \log(h) +$$

$$+ w \log(w)) + h\ w + \alpha_{FFT}^2\ h\ w \log(h\ w) + 2a) + (7a + 2a^2)\ h\ w.$$

One should add to this the execution of a Quick Sort on the full matrix to compute the best position. In the range of parameters in concrete applications (usually $6 \leq a \leq 30$ and $512 \leq h, w \leq 3000$), one can show that the computational cost is much less then that required by the optimal matching procedure (see Fig. 8).

With one fast calculation one can deduce both the matching coefficient and the rotation for any position of the fresco. This method can be applied in every case where one wants to localize a detail in a big scene up to relative rotation, brightness and contrast and it was also effective with very noisy data, proving its robustness (see following section).

4 Stability and numerical results

4.1 Pattern matching without noise

Extracting from a digital image G an *auto-fragment* f, i.e., a disk portion of a digital image which is rotated with respect to its original orientation, and applying the matching matrix $M(F,G)$, one can rearrange the entries of the matrix by decreasing values of the matching coefficient $|M(F,G)(i,j)|^2$. One wants that the first positions indicate the original position. Moreover, one would like also that the best positions can have matching coefficients clearly much bigger (discriminating power) then the others (wrong positions). Let us consider the function, say it *matching curve*, which maps each position into its matching coefficient, rearranged by decreasing values of the matching coefficient.

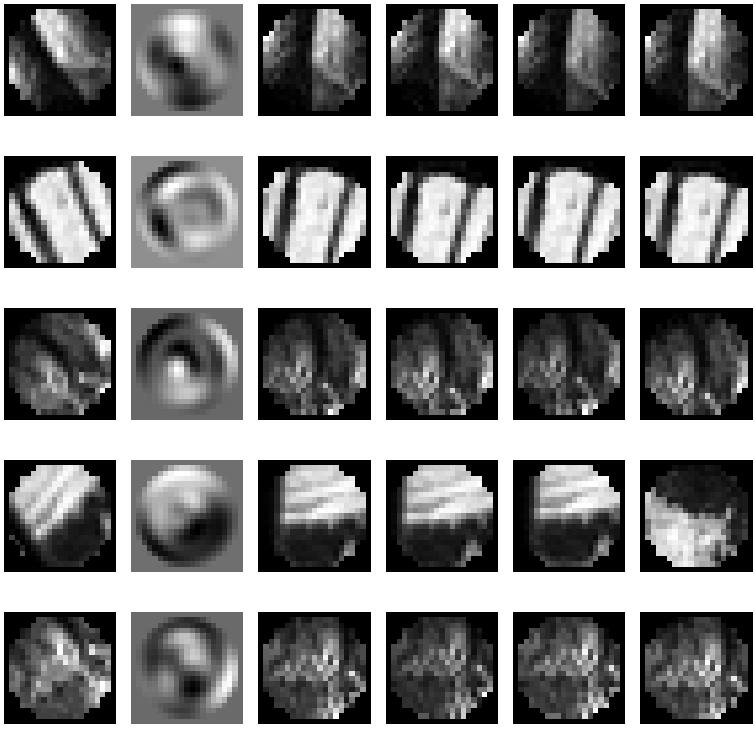

Fig. 9. Four best positions of a series of 5 auto-fragments are shown. The sample auto-fragments extracted from pictures of the fresco and rotated by $-37°$ are listed in the first column. In the second column the projection on the space $\mathcal{F}_{a,\varepsilon}$ and $m > 0$ of each fragment is presented. The last four columns show the best positions up to rotation with respect to the matching coefficient the algorithm is able to detect. They look very similar, but in fact they differ by the minimal displacement.

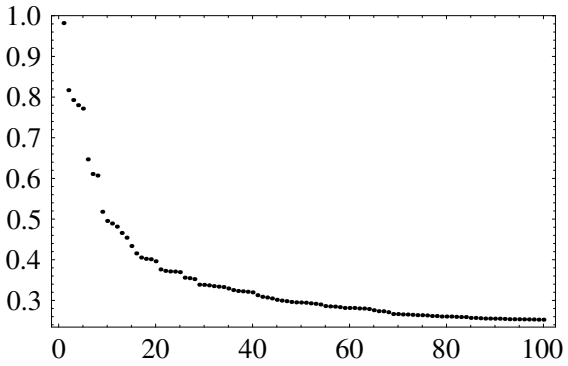

Fig. 10. Matching curve of an auto-fragment for the 100 first best positions. Each position is mapped into its corresponding matching coefficient.

Figures 9 and 10 show calculations of best positions applied on auto-fragments. For all tests that have been applied on auto-fragments extracted from 1000×1000 pixels random images, the method was successful in the 100% of the cases, in the sense that the first best position on the 1000000 possible competitors has always coincided with the original and the rates of decay in the first 10

positions were of order 1/5. Moreover, the calculation of the angle by means of $\arg(M(F,G)(i,j))$ is also correct, up to small errors, fast decreasing with increasing resolutions.

4.2 Real world cases: noise presence

In real world cases the comparison between images of the same object, but actually taken in different technical and time situations, can be made very difficult by presence of noise (or just by some strong differences as in the case of the fragments damaged by the bomb) and the correct order in the matching curve will be surely perturbed. We want to show now that the suggested (rotation) invariant (23) is quite robust in real world cases. The circular sum operator is responsible of the calculation of the matching matrix and one of the essential ingredients of the proposed method. Property (ii) of the circular sum is a specific and suggestive *auto-correcting property*: the errors δ_{α_k} on the angles at some k are compensated by the next term $k+1$ of the circular sum.

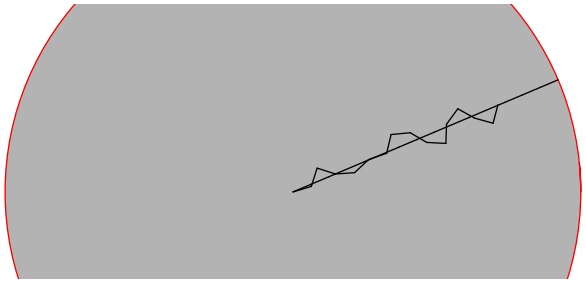

Fig. 11. Angles error compensation by the circular sum auto-correcting property. The straight line indicates the right angle and its length the right matching. A random error is added on each single term of the circular sum. The matching coefficient is reduced from 1 to 0.78.

One can make an analytic example in a very simplified case:

If $v_k = e^{ik\alpha}$, $k = 1, ..., m-2, m$ and $v_{m-1} = e^{i((m-1)\alpha+\delta_{\alpha_{m-1}})}$, it is not difficult to show that for m large enough and $\delta_\alpha \approx 0$

$$\bigoplus_{k=1}^{m} v_k \approx e^{i\alpha}\left((m-2) + e^{i\delta_{\alpha_{m-1}}} + e^{-i\delta_{\alpha_{m-1}}}\right). \tag{24}$$

This compensating effect is quite desirable in order to stabilize the angle calculation, while the reduction of the matching coefficient cannot be eliminated (see Fig. 11).

Motivated by the fast computation of the matching matrix and by the shown

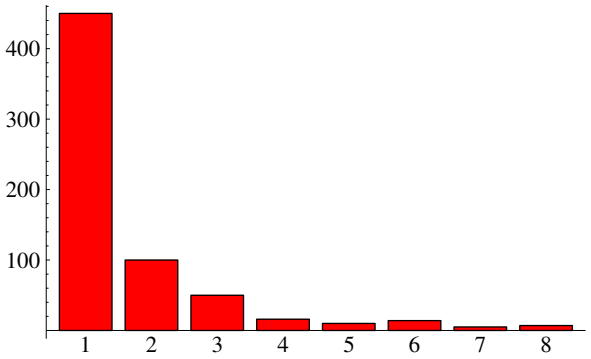

Fig. 12. Distribution of localized fragments with respect to the matching curve rank. *The 75% of the localized fragments were found in the first 3 best positions and the 90% in the first 20.* The total number of localized fragments is c.a. 800.

robustness, we have extensively applied the method on the real problem of the localization of fragments of the huge Andrea Mantegna's art fresco ("Stories of St. James and St. Christopher", 12 scenes of 15 m^2 each.). All fragments have been already tested on three of the scenes of 15 m^2 and we have detected the original position for 500-900 fragments on each. Some actual results are presented in Figures 4,6,7,12. In the experimentation, the first 100 best positions returned by the algorithm were considered and discussed by human operators. The calculation of a digitalized fragment of radius $a = 10$ pixels (equivalent to $2 - 3$ cm^2 real dimensions) on one scene of 3000×2400 pixels (equivalent to 15 m^2 real dimensions) takes actually about 120 seconds with a C/C++ implementation on a standard PC (AMD K7 Athlon 1 GHz, 500 MB RAM) with the FFTW library to compute discrete Fourier transforms.

4.3 Comparison with the ideal method in presence of noise

In this section, we want to compare the optimal matching procedure (Fig. 5) with the "circular sum procedure" (Fig. 11). Figure 13 shows the two methods in presence of noise: Montecarlo experiments of matching are applied on a random pattern with respect to itself, affected by white noise of increasing energy. In particular, the percentiles curves (0.05-0.5-0.95) related to matching coefficient and angle are depending essentially on the signal/noise (S/N) ratio and on the number of CH-moments used. For a fixed number of CH-moments (typically about 100), the methods look equivalent for ratio S/N$\geq$ 0.8 and they start to have some significant different behavior only for ratio S/N$<$ 0.8.

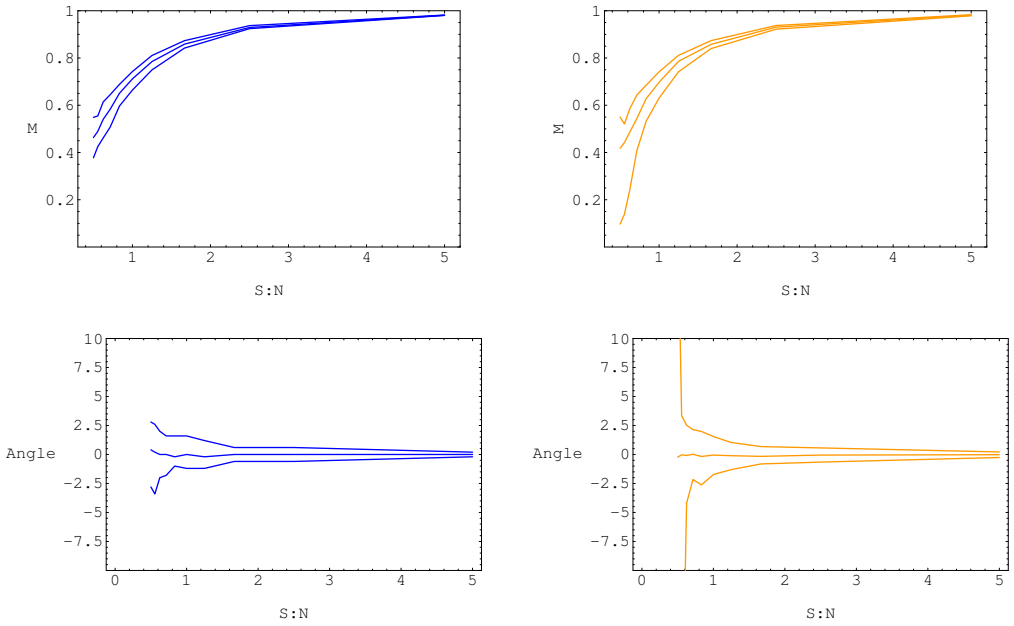

Fig. 13. Matching and angle percentiles (5% – 50% – 90%) curves for the optimal matching (left) and for the circular sum (right) procedures with respect to increasing S/N ratio.

4.4 Increasing discrimination power

The algorithm returns a sequence of positions ordered by means of the matching coefficient. In fact, the results of the experimentation on the fresco problem show that, for the 90% of the cases, one can reduce the analysis of the possible matching positions from $h \times w = 3000 \times 2400 = 7200000$ to the first 20 best ones only (Fig. 12). We want to exemplify how the discriminating power can be improved. In fact, one can extract from a fragment

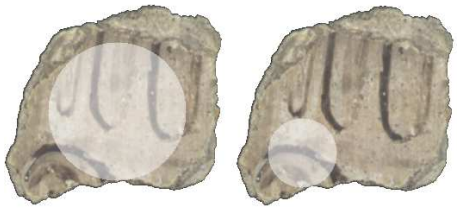

Fig. 14. Multiple disk selections extracted from the same fragment

more then one disk portion/selection. Given multiple sequences of best positions, maybe computed by the circular sum procedure on different selections, one can keep only those positions which are respecting the original mutual positions on the fragment and that have the same computed angle. Due to the robustness in detecting correct angles, a fast constraint check applied on the first 100 best positions returned by the circular sum procedure of the

Fig. 15. The original position on the fresco of the fragment shown in Fig. 14

two selections of the fragment in Fig. 14 reduced the coupled possible positions to 1 only: $p = (890, 1183)$ and $q = (884, 1189)$ with mutual distance $dist(p, q) = \sqrt{p^2 + q^2} \approx 8.48$ (pixels) while the mutual distance of the original selections (Fig. 14) is $dist(sel_1, sel_2) = \sqrt{sel_1^2 + sel_2^2} \approx 8.94$; the calculated angles are $\alpha_1 = 3.09$ and $\alpha_2 = 3.11$ (radiant). Therefore redundant calculations on a fragment ensure a very accurate detection of the original position of the fragment (Fig. 15) with high discriminating power.

An other way to improve the discrimination power is to combine our method with fast local registration [20] applied on the best positions returned by the algorithm. The list can consequently be reordered. In fact, fast registration algorithms based on optimization methods works when the images are already "close enough". Because of the robustness and the accuracy in angle detection, the fractional rigid rotation registration can be efficiently realized by using our algorithm. On the other hand, two digital images of the same object cannot in general be sampled exactly on the same grid. Some fractional shifts (or more complex elastic deformations) are usually present. One can simulate this effect by considering an image at resolution τ, shift it of one pixel, for example, in the right direction, and then scaling both, the original and the shifted, to resolution 2τ. The resulting images are representing the same object but in fact they differ of a fractional shift. Table 1 compares the output of our algorithm in a real case with its optimized version by local shift registration.

Match.	*Angle*	*Y*	*X*		*Match.*	*Angle*	*Y*	*X*
0.993	0.232	67	70		0.996	0.228	67	70
0.920	0.193	66	70		0.982	0.212	66	70
0.889	0.244	68	70		0.956	0.231	68	70
0.816	-2.904	**71**	**75**		0.940	0.233	**67**	**69**
0.795	-2932	**72**	**75**		0.934	0.224	**68**	**69**

Tab. 1. Matching, rotation angle and position computed on the same fragment before and after the fractional shift registration. In the optimized situation (right) by local registration one can appreciate the presence of a cluster of positions with matching coefficients very close and quite high. One can see that the first positions are preserved (with an improved matching and reduced variance in the angle computation), while the fourth and fifth incorrect positions are substituted by minimal displacements of the correct position.

Appendix

Notations and conventions

As we write $\tau > 0$ we mean $\tau = (\tau_1, ..., \tau_d) \in \mathbb{R}^d_+$; let we set also $w = (w_1, ..., w_d)$ where $w_i = C\tau_i^{-1}$ and $C > 0$ (C depends on the definition of the *Fourier transform*: usually $C = 1$ or $C = (2\pi)^{-1}$), $det(\tau) = \tau_1 ... \tau_d$ and $Q_w = \prod_{i=1}^d w_i[-\frac{1}{2}, \frac{1}{2})$. The multiplication $x \cdot y := xy := (x_1 y_1, ..., x_d y_d)$ of two vectors $x, y \in \mathbb{R}^d$ is assumed componentwise. If $f \in S'(\mathbb{R}^d)$ (the space of temperate distributions), $\hat{f}$ or $\mathcal{F}(f)$ stands for the *Fourier transform* of f. In particular, if f is summable function then

$$\mathcal{F}f(\omega) = \int_{\mathbb{R}^d} f(x) e^{-2\pi i \langle \omega, x \rangle_{\mathbb{R}^d}} dx,$$

where $\langle \cdot, \cdot \rangle_{\mathbb{R}^d}$ is the scalar product in $\mathbb{R}^d$. We denote $L^2(\mathbb{R}^d)$ the Lebesgue space of square summable functions. We consider the functions or distributions $\hat{\eta_f} = \hat{f}$ on Q_w and $\hat{\eta}_f = 0$ identically on $\mathbb{R}^d \backslash Q_w$, $\hat{\varepsilon_f} = \hat{f} - \hat{\eta}_f$ (the "tails" of $\hat{f}$ out of Q_w) and η_f, ε_f their respective inverse Fourier transforms. As we have fixed τ, we will write l^2 instead of $l^2(\tau\mathbb{Z}^d)$ the space of discrete signals with finite energy and we will suppose it endowed with the scalar product $\langle f, g \rangle_{l^2} \equiv det(\tau) \sum_{k \in \mathbb{Z}^d} f(\tau k) \overline{g(\tau k)}$. If f is a discrete signal then we will denote with $\mathcal{F}f$ or $\hat{f}$ also the *discrete Fourier transform* of f. For any function (on continuous or discrete domain) h we define $h^*(x) = h(-x)$ and $I(h) = \overline{h^*}$ the involution operator and with $f * g$ the convolution operator of f and g.

Error Analysis in Sampling Theory

For the sake of completeness, we recall some of the results in [12] for (aliasing) error analysis in moment integration.

In particular, let us introduce some of the properties of *Wiener amalgam spaces* we will use in the following without introducing them in full generality.

For a more complete description of these spaces see [19]. We use Wiener amalgam spaces because of their important capability of highlighting the relations between continuous and discrete behaviors of functions under the action of sampling.

Given a relatively compact set $\Omega \subset \mathbb{R}^d$, a Partition of the Unity $\Psi = (\psi_k)_{k\in\mathbb{Z}^d}$, such that $\mathrm{supp}(\psi_k) \subset \tau k + \Omega$, a Banach space of functions $(B, \|\cdot\|_B)$ such that

$$\|\psi_k f\|_B \leq C\|f\|_B, \quad \forall f \in B,$$

and w a discrete weight function, we define the Wiener amalgam space as:

$$W(\Psi, B, l^q_w) = \{f \in S' : f\psi_k \in B \quad \forall k \in \mathbb{Z}^d, (\|f\psi_k\|_B)_{k\in\mathbb{Z}^d} \in l^q_w(\mathbb{Z}^d)\}.$$

Moreover, one can define the norm:

$$\|f|W(B, l^q_w)\| \equiv \left(\sum_{k\in\mathbb{Z}^d} \|f\psi_k\|^q_B w(k)^q\right)^{1/q}.$$

With this norm the space $(W(\Psi, B, l^q_w), \|\cdot|W(B, l^q_w)\|)$ is a Banach space.

When the weight function w is assumed moderate, that is $w(x+y) \leq w(x)(1+|y|)^s$ for all $x, y \in \mathbb{R}^d$ and some $s \geq 0$, then one can show that $W(\Psi, B, l^q_w) \equiv W(B, l^q_w)$ does not depend on the particular Ψ taken.

Theorem 1 *(Useful properties)*

i) If $B^1_{loc} \subset B^2_{loc}$ *and* $l^{q_1}_{w_1} \subset l^{q_2}_{w_2}$ *then* $W(B^1, l^{q_1}_w) \subset W(B^2, l^{q_2}_w)$ *continuously;*
ii) $\mathcal{F}(W(L^p, l^q)) \subset W(L^{q'}, l^{p'})$ *continuously, for* $1 \leq p, q \leq 2$, $1/p + 1/p' = 1$ *and* $1/q + 1/q' = 1$.

The *aliasing error* [21] can be measured as the (Wiener amalgam) norm of the "tails" $\mathcal{F}\varepsilon_f$ of the Fourier transform of a function f and it stands for the uncertainty one has in identifying the function defined on a continuous domain from its samples on a regular or irregular set of nodes. One can consider aliasing errors as an estimate of the ambiguity with which one manages functions or samples. From the Whittacker-Shannon theorem is immediate to show that for all $f \in L^2 \cap C^0$ and any $\tau > 0$ such that $f_{|\tau\mathbb{Z}^d} \in l^2$:

$$f(x) = \sum_{k\in\mathbb{Z}^d} (f(\tau k) - \varepsilon_f(\tau k)) \prod_{i=1}^{d} sinc(\tau_i^{-1} x_i - k_i) + \varepsilon_f(x). \tag{25}$$

The quantities ε_f are the uncertainty on the reconstruction of f directly from its samples. In fact, for band-limited functions $\varepsilon_f \equiv 0$ and formula (25) reduces to the well known Whittacker-Shannon theorem. In particular in $L^2(\mathbb{R}^d)$ the

reconstruction ambiguity on functions propagates to their scalar products as we will show in the following results.

Lemma 2 *One has the following properties:*

i) The identity is continuous from $W(C^0, l^2)$ *to* $L^2 \cap C^0$, *i.e.* $\forall f \in W(C^0, l^2)$ $\exists \quad C > 0$ *such that* $\|f\|_2 \leq C\|f|W(C^0, l^2)\|$;

ii) For each τ, $0 < \tau \leq \tau_0$, $\exists \quad C_0 > 0$, *not depending on the resolution, such that* $\forall f \in W(C^0, l^2)$ $\|f_{|\tau Z^d}\|_{l^2} \leq C_0\|f|W(C^0, l^2)\|$.

Theorem 3 *For* $f, g \in L^2 \cap C^0$, *assume* $\mathcal{F}f, \mathcal{F}g \in W(L^2, l^1)$ *and* $\tau > 0$ *fixed. Then* $f, g \in W(C^0, l^2)$, *and we can approximate the* L^2-*scalar product of* f *and* g *as follows:*

$$\begin{aligned} &|\langle f, g\rangle_{L^2} - \langle f_{|\tau Z^d}, g_{|\tau Z^d}\rangle_{l^2}| \leq \\ &\leq C_1\|f\| \cdot \|\varepsilon_g\| + C_2\|g\| \cdot \|\varepsilon_f\| + C_3\|\varepsilon_f\| \cdot \|\varepsilon_g\|. \end{aligned} \tag{26}$$

where the norms on the right side are taken in $W(C^0, l^2)$.

PROOF. Observe that, by Lemma 3 ii), f and g are such that $f_{|\tau\mathbb{Z}^d} \in l^2(\tau\mathbb{Z}^d)$and $g_{|\tau\mathbb{Z}^d} \in l^2(\tau\mathbb{Z}^d)$ for all $\tau > 0$. By using (25) it's easy to show that it holds the following inequality:

$$\begin{aligned} &|\langle f, g\rangle_{L^2} - \langle f_{|\tau Z^d}, g_{|\tau Z^d}\rangle_{l^2}| \leq \\ &\leq \|\varepsilon_f\|_{l^2}\|g\|_{l^2} + \|\varepsilon_g\|_{l^2}\|f\|_{l^2} + \|\varepsilon_f\|_{l^2}\|\varepsilon_g\|_{l^2} + \|\varepsilon_f\|_{L^2}\|\varepsilon_f\|_{L^2}. \end{aligned} \tag{27}$$

(use the orthogonality of the sequence $(\prod_{i=1}^d sinc(\tau_i^{-1}x_i - k_i))_{k\in\mathbb{Z}^d}$ and the Cauchy-Schwarz inequality). It will be enough to realize that $\mathcal{F}\varepsilon_f$ and $\mathcal{F}\varepsilon_g$ are in $W(L^2, l^1)$, hence by ii) of Theorem 1 also ε_f and ε_g are in $W(C^0, l^2)$ and apply the previous i) and ii) of the Lemma 2. This concludes the proof.

Acknowledgments

The authors want to thank Claudio Fanin (Istituto Nazionale di Fisica Nucleare, sezione di Padova, Italy) and Giuseppe Galeazzi (Department of Physics "G. Galilei", University of Padova, Italy) for the fruitful cooperation and their valuable suggestions during the preparation of this work. The authors are indebt with Rocco Cazzato and Germano Costa for the technical support and the management of the Mantegna Laboratory (University of Padova), during the experimental part of the work.

References

[1] S. T. Ali, J. P. Antoine, J. P. Gazeau, *Coherent States, Wavelets and their Generalizations*, Springer-Verlag, 2000.

[2] J.-P. Antoine, P. Vandergheynst, and R. Murenzi, Two-dimensional directional wavelets in image processing. Int. J. Imag. Syst. Tech, 7 (1996), 152-165.

[3] H. H. Arsenault, Y. N. Hsu, and K. Chalasinska-Macukow, Rotation-invariant pattern recognition, Opt. Eng. 23 (1984) 705-709.

[4] H. H. Arsenault, and C. Belisle, Contrast-invariant pattern recognition using Circular Harmonic components, Appl. Opt. 24 (1985) 2072-2075.

[5] H. H. Arsenault, Y. Sheng, Properties of the Circular Harmonic expansion for rotation invariant pattern recognition, Appl. Opt. 25 (18) (1986), 3225-3229.

[6] H. H. Arsenault, D. Asselin, D. Prevost, L. Leclerc, and Y. Sheng, New ways of using optics for faster pattern recognition, Proc. SPIE 1806 (1993) 314-322.

[7] M. Carli, G. Jacovitti, A. Neri, Pattern recognition and location based on the Gauss-Laguerre Transform, Proc. SPIE Multimedia System and Applications III, 5-8 November 2000, Boston, Massachusetts USA.

[8] I. Daubechies, *Ten Lectures on Wavelets*, Philadelphia, Society for Industrial and Applied Mathematics, 1992.

[9] H. G. Feichtinger, T. Strohmer (eds), *Gabor Analysis and Algorithms*, Birkhäuser, 1998.

[10] M. Fornasier, *Un Metodo per la Rappresentazione ed il Confronto di Immagini a Meno di Rotazione* (Italian), Diploma thesis, University of Padova, Oct. 1999.

[11] M. Fornasier, Decompositions of Hilbert spaces: local construction of global frames, Proc. Int. Conf. "Constructive theory of functions", Varna 2002, (B. Bojanov, Ed.), DARBA, Sofia, 2003, pp. 275-281.

[12] M. Fornasier, Function spaces inclusions and rate of convergence of Riemann-type sums in numerical integration, Numerical Functional Analysis and Opt., 2, Vol. (1 & 2), 2003, pp. 45-57.

[13] M. Fornasier, *Constructive Methods for Numerical Applications in Signal Processing and Homogenization Problems*, Ph.D. thesis, University of Padova, Dec. 2002.

[14] M. Fornasier, Quasi-orthogonal decompositions of structured frames, J. Math. Anal. Appl., Vol. 289, Issue 1 , 1 January 2004, pp. 180-199.

[15] G. Galeazzi, D. Toniolo, I frammenti della Chiesa degli Eremitani: un approccio matematico alla soluzione del problema (Italian), Atti del convegno "Filosofia e Tecnologia del restauro", gli 'Emblémata', Abbazia di Praglia, Oct. 1994, pp. 89-97.

[16] G. Galeazzi, D. Toniolo, Il problema della ricostruzione degli affreschi della Chiesa degli Eremitani in Padova. (Italian), Atti del convegno "Il complesso basilicale di San Francesco di Assisi ad un anno dal terremoto", Assisi 24-26 Sept. 1998.

[17] K. Gröchenig, *Foundation of Time-Frequency Analysis*, Birkhäuser Verlag, 2001.

[18] J. Gu, H. Z. Shu, C. Toumoulin, L.M. Luo, A novel algorithm for fast computation of Zernike moments, Pattern Recognition 35 (12)(2002), 2905-2911.

[19] C. Heil, An introduction to weighted Wiener amalgams, Proc. Int. Conf. on Wavelets and their Applications (Chennai, January 2002), R. Ramakrishnan and S. Thangavelu, eds, Allied Publishers, New Delhi, to appear 2003.

[20] J. Kybic, M. Unser, Fast parametric elastic image registration, IEEE Transactions on Image Processing, to appear.

[21] A. Papoulis, *Signal analysis*, New York etc.: McGraw-Hill Book Company. XI, 1977.

[22] E. P. Simoncelli, A rotation-invariant pattern signature, Third Int'l Conference on Image processing, Lausanne, Switzerland, September 1996.

[23] A. Stoschek, T. P. Y. Yu, R. Hegerl, Rotation-invariant and robust multiple-2D-object detection using steerable pyramid denoising and optimized Circular Harmonic filters, Proc. of 13^{th} Int. Conf. on Pattern Recogn. 1996, Wien, IEEE Comp. Soc. Press, Vol. 2, Track B., pp. 376-380.

[24] R. Murenzi, *Ondelettes Multidimensionelles et Applications à l'Analyse d'Images*, Ph.D. thesis, Univ. Cath. Luovain, Luovain-la-Neuve, 1990.

[25] D. Toniolo, M. Fornasier, Computer-based recomposition of the frescoes in the Ovetari Chapel in the Church of the Eremitani in Padua. Methodology and initial results, (English/Italian), in "Mantegna nella chiesa degli Eremitani a Padova. Il recupero possibile" Ed. Skira, May 2003, pp. 15-23.

[26] G. N. Watson, *Theory of Bessel Functions*, Cambridge University Press, 1966.

[27] K. B. Wolf, *Integral Transforms in Science and Engineering*, Mathematical Concepts and Methods in Science and Engineering, Vol. 11. New York, London: Plenum Press. XIII, 1979.

Vitae

Massimo Fornasier received his Ph.D degree in Computational Mathematics on February 2003 at the University of Padova, Italy. Within the European network RTN HASSIP (Harmonic Analysis and Statistics for Signal

and Image Processing) HPRN-CT-2002-00285, he cooperated as PostDoc with NuHAG (the Numerical Harmonic Analysis Group), Department of Mathematics of the University of Vienna, Austria and the AG Numerical/Wavelet-Analysis Group of the Department of Mathematics and Computer Science of the Philipps-University in Marburg, Germany (2003). He is currently research assistant at the Department of Mathematical Methods and Models for the Applied Science at the University "La Sapienza" in Rome. His research interests include applied harmonic analysis with particular emphasis on time-frequency analysis and decompositions for applications in signal and image processing. Since 1998, he developed with Domenico Toniolo the Mantegna Project (http://www.pd.infn.it/∼labmante/) at the University of Padova and the local laboratory for image processing and applications in art restoration.

Domenico Toniolo received his Doctoral degree in Electric and Electronic Engeneering on March 1960 at the University of Padova, Italy. He developed most of his scientific activity at *Istituto Nazionale di Fisica Nucleare* (INFN) Laboratory in Legnaro (Italy), working on experiments of diffusion of fast neutrons, where he was in charge of both the experiment realizations and the theoretical data analysis of signals and measures. From 1964 until 1969 he was Professor of Electronics for Physics students. Since 1970 he has been Professor of General Physics at the Engeneering faculty of the University of Padova. In 1994 he started the realization of the Mantegna Project, an attempt of computer-based reconstruction of the art frescoes in the Eremitani Church (Padova, Italy), fragmented by a bombing in the Second World War (1944).